Determination of nuclear parton distribution functions and their uncertainties at next-to-leading order

M. Hirai,[1,2] S. Kumano,[2,3] and T.-H. Nagai[3]

[1]*Department of Physics, Tokyo Institute of Technology, Ookayama, Meguro-ku, Tokyo, 152-8550, Japan*

[2]*Institute of Particle and Nuclear Studies, High Energy Accelerator Research Organization (KEK), 1-1, Ooho, Tsukuba, Ibaraki, 305-0801, Japan*

[3]*Department of Particle and Nuclear Studies, Graduate University for Advanced Studies, 1-1, Ooho, Tsukuba, Ibaraki, 305-0801, Japan*

(Received 18 September 2007; published 19 December 2007)

Nuclear parton distribution functions (NPDFs) are determined by global analyses of experimental data on structure-function ratios $F_2^A/F_2^{A'}$ and Drell-Yan cross-section ratios $\sigma_{DY}^A/\sigma_{DY}^{A'}$. The analyses are done in the leading order (LO) and next-to-leading order (NLO) of running coupling constant α_s. Uncertainties of the NPDFs are estimated in both LO and NLO for finding possible NLO improvement. Valence-quark distributions are well determined, and antiquark distributions are also determined at $x < 0.1$. However, the antiquark distributions have large uncertainties at $x > 0.2$. Gluon modifications cannot be fixed at this stage. Although the advantage of the NLO analysis, in comparison with the LO one, is generally the sensitivity to the gluon distributions, gluon uncertainties are almost the same in the LO and NLO. It is because current scaling-violation data are not accurate enough to determine precise nuclear gluon distributions. Modifications of the PDFs in the deuteron are also discussed by including data on the proton-deuteron ratio F_2^D/F_2^p in the analysis. A code is provided for calculating the NPDFs and their uncertainties at given x and Q^2 in the LO and NLO.

DOI: 10.1103/PhysRevC.76.065207 PACS number(s): 13.60.Hb, 12.38.−t, 24.85.+p, 25.30.−c

I. INTRODUCTION

Cross sections of high-energy nuclear reactions are expressed in terms of nuclear parton distribution functions (NPDFs), so precise NPDFs are essential for finding any new phenomena in the high-energy reactions. Recently, this topic is becoming important in heavy-ion collisions for investigating properties of quark-hadron matters [1] and also in neutrino reactions for investigating neutrino-oscillation physics [2]. Determination of precise NPDFs is valuable for studying various phenomena in heavy-ion reactions such as color glass condensate [3], J/ψ suppression [4], and parton-energy loss [5]. The NPDF studies should be also important for heavy-ion collisions at LHC (Large Hadron Collider) [6].

In neutrino oscillation experiments, most data are taken at small $Q^2 (< 1\text{GeV}^2)$. We could approach such a kinematical region from the high-energy deep inelastic one by using quark-hadron duality [7]. However, there are still unresolved issues in neutrino deep inelastic scattering. For example, an anomalous $\sin^2\theta_W$ value was reported in the neutrino-iron scattering by the NuTeV Collaboration [8]. It could be related to a nuclear modification difference between the parton distributions u_v and d_v [9–11] because the iron target is used in the NuTeV measurements. There is also an issue that nuclear corrections are different from the ones expected from electron and muon scattering experiments according to recent NuTeV data [12].

In these high-energy nuclear reactions, nucleonic PDFs rather than the nuclear ones are often used in calculating cross sections by neglecting nuclear modifications although it is well known that nuclear corrections could be as large as 20% in medium-size nuclei [13]. These nuclear modifications have been experimentally investigated mainly by the measurements of structure-function ratios $F_2^A/F_2^{A'}$ and Drell-Yan cross-section ratios $\sigma_{DY}^A/\sigma_{DY}^{A'}$. Physical mechanisms of the nuclear corrections are, for example, summarized in Ref. [13]. In the small-x region, the NPDFs become smaller than the corresponding nucleonic ones, which is called shadowing. There are depletions at medium x, which is related to the nuclear binding mechanism and possibly to a nucleonic modification inside a nuclear medium [14]. At large x, the nucleon's Fermi motion gives rise to positive corrections.

Because the PDFs are related to the nonperturbative aspect of quantum chromodynamics (QCD), theoretical calculations have been done by lattice QCD or phenomenological models. However, such calculations are not accurate enough at this stage. One would like to have accurate NPDFs, which are obtained in a model-independent way, for calculating precise nuclear cross sections. We should inevitably rely on experimental data for determining them.

Studies of nucleonic PDFs have a long history with abundant experimental data in a wide kinematical region [15]. However, determination of NPDFs is still at a premature stage with the following reasons. First, available experimental data are limited. The experiments of the Hadron-Electron Ring Accelerator (HERA) provided data for structure functions at small x in a wide range of Q^2; however, such data do not exist for nuclei. Because of final-state interactions, hadron-production data may not be suitable for the NPDF determination, whereas they are used in the nucleonic analysis. Second, the analysis technique is not established. Parametrization studies for the NPDFs started only recently. The NPDFs are expressed in terms of a number of parameters that are then determined by a χ^2 analysis of the nuclear data. However, it is not straightforward to find functional forms of mass-number (A) and Bjorken-x dependencies in the NPDFs. Furthermore, higher-twist effects could be important in the small-Q^2 region.

A useful parametrization was investigated in Ref. [16] by analyzing F_2 structure functions and Drell-Yan data;

however, the distributions were obtained by simply assigning appropriate parameter values by hand in the versions of 1998 and 1999. The first χ^2 analysis was reported in Ref. [17], and then uncertainties of the NPDFs were obtained [18]. All of these analyses are done in the leading order (LO) of the running coupling constant α_s. A next-to-leading-order (NLO) analysis was recently reported [19]. The LO χ^2 analysis with the uncertainties was also investigated in the 2007 version of Ref. [16]. There are related studies on the nuclear shadowing [20–22] and a global analysis of structure functions [23].

In this way, the parametrization studies have been developed recently for the NPDFs, and they are not sufficient. Here, we extend our studies in Refs. [17,18] by focusing on the following points:

(i) NLO analysis with NPDF uncertainties together with a LO one,
(ii) roles of NLO terms on the NPDF determination by comparing LO and NLO results,
(iii) better determination of x and A dependence,
(iv) nuclear modifications in the deuteron by including $F_2(\text{deuteron})/F_2(\text{proton})$ data,
(v) flavor asymmetric antiquark distributions.

This article is organized as follows. In Sec. II, our analysis method is described for determining the NPDFs. Analysis results are explained in Sec. III. Nuclear modifications in the deuteron are discussed in Sec. IV. The results are summarized in Sec. V.

II. ANALYSIS METHOD

The optimum NPDFs are determined by analyzing experimental data of the F_2 structure functions and Drell-Yan cross sections for nuclear targets. Details of our analysis method are described in Refs. [17,18], so only the outline is explained in the following.

A. Parametrization

The parton distribution functions are expressed by two variables x and Q^2. The variable Q^2 is defined $Q^2 = -q^2$ with the virtual photon momentum q in the lepton scattering, and the scaling variable x is given by $x = Q^2/(2M\nu)$ with the nucleon mass M and the energy transfer ν. The variables for the Drell-Yan process are momentum fractions, x_1 and x_2 for partons in the projectile and target, respectively, and Q^2 defined by the dimuon mass as $Q^2 = m^2_{\mu\mu}$. In our analysis, the NPDFs are expressed in terms of corresponding nucleonic PDFs multiplied by weight functions:

$$f_i^A\left(x, Q_0^2\right) = w_i(x, A, Z) f_i\left(x, Q_0^2\right). \tag{1}$$

The functions f_i^A and f_i indicate type-i NPDF and nucleonic PDF, respectively, and w_i is a weight function that indicates a nuclear modification for the type-i parton distribution. The function w_i generally depends on not only x and A but also the atomic number Z. It should be noted that this expression sacrifices the large-x (>1) nuclear distributions. Finite distributions exist even at $x > 1$ in nuclei, whereas the distributions should vanish in the nucleon.

Flavor symmetric antiquark distributions are assumed for $\bar{u}$, $\bar{d}$, and $\bar{s}$ in the previous analyses [17,18]. From the violation of the Gottfried sum rule and Drell-Yan measurements, it is now well known that these antiquark distributions are different [24]. It is more natural to investigate modifications from the flavor asymmetric antiquark distributions in the nucleon. In this work, flavor asymmetric antiquark distributions are used in nuclei, and the distribution type i indicates u_v, d_v, $\bar{u}$, $\bar{d}$, $\bar{s}$, and g:

$$\begin{aligned}
u_v^A\left(x, Q_0^2\right) &= w_{u_v}(x, A, Z)\frac{Zu_v\left(x, Q_0^2\right) + Nd_v\left(x, Q_0^2\right)}{A},\\
d_v^A\left(x, Q_0^2\right) &= w_{d_v}(x, A, Z)\frac{Zd_v\left(x, Q_0^2\right) + Nu_v\left(x, Q_0^2\right)}{A},\\
\bar{u}^A\left(x, Q_0^2\right) &= w_{\bar{q}}(x, A, Z)\frac{Z\bar{u}\left(x, Q_0^2\right) + N\bar{d}\left(x, Q_0^2\right)}{A},\\
\bar{d}^A\left(x, Q_0^2\right) &= w_{\bar{q}}(x, A, Z)\frac{Z\bar{d}\left(x, Q_0^2\right) + N\bar{u}\left(x, Q_0^2\right)}{A},\\
\bar{s}^A\left(x, Q_0^2\right) &= w_{\bar{q}}(x, A, Z)\bar{s}\left(x, Q_0^2\right),\\
g^A\left(x, Q_0^2\right) &= w_g(x, A, Z) g\left(x, Q_0^2\right),
\end{aligned} \tag{2}$$

whereas the relation $\bar{u}^A = \bar{d}^A = \bar{s}^A$ is assumed in Refs. [17,18]. The number of flavor is three (four) at $Q^2\langle m_c^2(Q^2) m_c^2\rangle$ [18]. The bottom and top quark distributions are neglected. The strange-quark distributions are assumed to be symmetric ($s = \bar{s}$), although there are recent studies on possible asymmetry $s \neq \bar{s}$ [25]. The charm-quark distributions are created by Q^2 evolution effects [18]. As for the nucleonic PDFs in the LO and NLO, the MRST (Martin, Roberts, Stirling, and Thorne) parametrization of 1998 is used [26] in this analysis, where the charm-quark mass is $m_c = 1.35$ GeV and scale parameters are $\Lambda_4 = 0.174$ and 0.300 GeV for the LO and NLO, respectively. In our previous analysis [18], the MRST-2001 version was employed. Because the NLO gluon distribution is negative at x <0.005 and $Q^2 = 1$ GeV^2 in the 2001 version, we use the 1998 parametrization in this work. Negative gluon distributions in nuclei could affect our analysis inappropriately in the shadowing region. Furthermore, other researchers may use our NPDFs at small x (<0.005) with $Q^2 \sim 1$ GeV^2 for calculating cross sections, for example, in LHC experiments. We tested various PDFs of the nucleon, but overall results are not significantly changed. Because we are interested in obtaining the distributions at $Q^2 \geqslant 1$ GeV^2 in comparison with other distributions and also our previous distributions, we decided to use the MRST distributions. In the analyses of the CTEQ (Coordinated Theoretical/Experimental Project on QCD Phenomenology and Tests of the Standard Model) Collaboration, the initial scale $Q^2 = (1.3)^2$ GeV^2 is used.

The nuclear modification is assumed to have the following functional form:

$$w_i(x, A, Z) = 1 + \left(1 - \frac{1}{A^\alpha}\right)\frac{a_i + b_i x + c_i x^2 + d_i x^3}{(1-x)^{\beta_i}}, \tag{3}$$

where α, a_i, b_i, c_i, d_i, and β_i are parameters. The parameter a_i controls the shadowing part; b_i, c_i, and d_i determine a minute functional form; and β_i is related to the Fermi-motion part at large x. The parameter β_i is fixed at $\beta_i = 0.1$ because it cannot be determined from a small number of data in the Fermi-motion part. As it will be shown in the result section, the antiquark and gluon modifications cannot be determined from the present data at $x > 0.3$. If a large β_i, for example, $\beta_i = 1$, is taken, the antiquark and gluon distributions could become unrealistically large at large x. To avoid such an issue, $\beta_i = 0.1$ is used. The overall A dependence in Eq. (3) is taken $\alpha = 1/3$ simply by considering nuclear volume and surface contributions [27]. There are three constraints for the parameters by the nuclear charge Z, baryon number A, and momentum conservation [17,18,28]:

$$\begin{aligned} Z &= \int dx \frac{A}{3}\left[2u_v^A(x,Q_0^2) - d_v^A(x,Q_0^2)\right], \\ A &= \int dx \frac{A}{3}\left[u_v^A(x,Q_0^2) + d_v^A(x,Q_0^2)\right], \\ A &= \int dx A x\left[u_v^A(x,Q_0^2) + d_v^A(x,Q_0^2) + 2\left\{\bar{u}^A(x,Q_0^2)\right.\right. \\ &\quad \left.\left. + \bar{d}^A(x,Q_0^2) + \bar{s}^A(x,Q_0^2)\right\} + g^A(x,Q_0^2)\right]. \end{aligned} \tag{4}$$

We selected three parameters, a_{u_v}, a_{d_v}, and a_g, which are determined by these conditions.

Following improvements are made from the previous analysis [18]. First, the parametrization of x dependence is modified. The meaning of the parameters b_i, c_i, and d_i is not obvious, so it is difficult to limit the ranges of these parameters in the analysis. Here, we take x points (x_{0i}^+, x_{0i}^-) of extreme values for the function $a_i + b_i x + c_i x^2 + d_i x^3$ as the parameters instead of b_i and c_i. They are related with each other by

$$b_i = 3d_i x_{0i}^+ x_{0i}^-, \quad c_i = -\frac{3d_i}{2}(x_{0i}^+ + x_{0i}^-). \tag{5}$$

Then, the values of x_{0i}^+ and x_{0i}^- become transparent at least for the valence-quark distributions. From the measurements of the ratios F_2^A/F_2^D, where D indicates the deuteron, we have a rough idea that the extreme values should be $x_{0v}^- \sim 0.15$ and $x_{0v}^+ \sim 0.6$. The Drell-Yan measurements indicate $x_{0\bar{q}}^- \sim 0.1$ for the antiquark distributions. The value $x_{0\bar{q}}^+$ and the extreme values for the gluon distribution are not obvious.

Second, the A dependence $1/A^{1/3}$ is too simple. From gross nuclear properties, the leading A dependence could be described by $1 - 1/A^{1/3}$. To describe more details, the parameters d_v, $a_{\bar{q}}$, $d_{\bar{q}}$, and d_g are taken to be A dependent:

$$\eta = \eta^{(1)}\left(1 - \frac{1}{A^{\eta^{(2)}}}\right), \quad \eta = d_v, \quad a_{\bar{q}}, \quad d_{\bar{q}}, \quad d_g. \tag{6}$$

Because the extreme values x_{0i}^+ and x_{0i}^- are almost independent of A according to the F_2 data and also from the previous analyses [17,18], they are assumed to be independent of A. In addition, the parameters $d_{\bar{q}}^{(1)}$ and x_{0g}^- are fixed in the antiquark and gluon distributions as follows. Because the gluon distributions cannot be well determined from the present data, the parameter c_g is taken $c_g = 0$ as assumed in the previous analysis [18]. It means that x_{0g}^- and x_{0g}^+ are related by $x_{0g}^- = -x_{0g}^+$ from Eq. (5). There are still six parameters for the antiquark distributions and they should be too many in comparison with four parameters for the valence-quark distributions. We decided to fix the parameter $d_{\bar{q}}^{(1)}$, which is sensitive to the gluon shadowing ratio to the antiquark one because of the momentum conservation. We found that the gluon shadowing cannot be well determined even in the NLO analysis; therefore, the value of $d_{\bar{q}}^{(1)}$ is taken so that the gluon shadowing is similar to the antiquark shadowing.

After all, the following 12 parameters are used for expressing the nuclear modifications:

$$\begin{array}{lllllll} \text{valence quark:} & x_{0v}^+, & x_{0v}^-, & d_v^{(1)}, & d_v^{(2)}, & & \\ \text{antiquark:} & x_{0\bar{q}}^+, & x_{0\bar{q}}^-, & a_{\bar{q}}^{(1)}, & a_{\bar{q}}^{(2)}, & d_{\bar{q}}^{(2)}, & \\ \text{gluon:} & x_{0g}^+, & d_g^{(1)}, & d_g^{(2)}. & & & \end{array} \tag{7}$$

These parameters are determined by the following global analysis.

B. Experimental data

Most of used experimental data are explained in Ref. [18]. First, the data for F_2^A/F_2^D are from European Muon Collaboration (EMC) [29–31]; the SLAC (Stanford Linear Accelerator Center)-E49, E87, E139, and E140 Collaborations [32–35]; the Bologna-CERN-Dubna-Munich-Saclay (BCDMS) Collaboration [36,37]; the New Muon Collaboration (NMC) [38]; the Fermilab (Fermi National Accelerator Laboratory)-E665 Collaboration [39,40]; and the HERMES [41]. Second, the ratios $F_2^{A_1}/F_2^{A_2}$ $(A_2 \neq D)$ are from the NMC [38,42,43]. Third, the Drell-Yan data are from the Fermilab-E772 [44] and E866/NuSea [45] Collaborations.

Additional data to the HKN04 (Hirai, Kumano, Nagai in 2004) analysis are the ones for the deuteron-proton ratio F_2^D/F_2^p. These deuteron data are added because precise nuclear modifications are needed for the deuteron that is, for example, used in heavy-ion experiments at the Relativistic Heavy Ion Collider (RHIC) [1]. The F_2^D/F_2^p data are taken from the measurements by the EMC [46], the BCDMS [47], the Fermilab-E665 [48], and the NMC [49]. These data are used for extracting information on the flavor asymmetric antiquark distributions $(\bar{u} \neq \bar{d})$ in the nucleon [24]. Therefore, the flavor asymmetric antiquark distributions in Eq. (2) are essential for a successful fit and for extracting information on modifications in the deuteron.

Because the DGLAP (Dokshitzer-Gribov-Lipatov-Altarelli-Parisi) evolution can be applied only in the perturbative QCD region, the data with small Q^2 values cannot be used in the analysis. However, the data in a relatively small-Q^2 region ($Q^2 = 1$–3 GeV^2) are valuable for determining antiquark distributions at small x ($x = 0.001$–0.01). As a compromise of these conflicting conditions, only the data with $Q^2 \geqslant 1$ GeV^2 are used in the analysis. However, one should note that the data in the range $Q^2 = 1$–3 GeV^2 may contain significant contributions of higher-twist effects that are not considered in our leading-twist analysis.

C. χ^2 analysis

The parameters are determined by fitting experimental data for the ratios of the structure functions F_2^A and Drell-Yan cross sections. The total χ^2

$$\chi^2 = \sum_j \frac{\left(R_j^{\rm data} - R_j^{\rm theo}\right)^2}{\left(\sigma_j^{\rm data}\right)^2}, \tag{8}$$

is minimized to obtain the optimum parameters. The ratio $R_j^{\rm data}$ indicates experimental data for $F_2^A/F_2^{A'}$ and $\sigma_{DY}^{pA}/\sigma_{DY}^{pA'}$, and $R_j^{\rm theo}$ is a theoretical ratio calculated by the parametrized NPDFs. The initial scale Q_0^2 is taken $Q_0^2 = 1$ GeV^2, and the distributions in Eq. (2) are evolved to experimental Q^2 points to calculate the χ^2 by the DGLAP evolution equations [50]. All the calculations are done in the LO or NLO, and the modified minimal subtraction ($\overline{\rm MS}$) scheme is used in the NLO analysis.

The structure function $F_2^A(x, Q^2)$ is expressed in terms of the NPDFs and coefficient functions:

$$F_2^A(x, Q^2) = \sum_{i=1}^{n_f} e_i^2 x \Big\{ C_q(x, \alpha_s) \otimes \left[q_i^A(x, Q^2) + \bar{q}_i^A(x, Q^2)\right] + C_g(x, \alpha_s) \otimes g^A(x, Q^2) \Big\}, \tag{9}$$

where $C_q(x, \alpha_s)$ and $C_g(x, \alpha_s)$ are the coefficient functions [51] and e_i is a quark charge. The symbol $\otimes$ denotes the convolution integral:

$$f(x) \otimes g(x) = \int_x^1 \frac{dy}{y} f\left(\frac{x}{y}\right) g(y). \tag{10}$$

The proton-nucleus Drell-Yan cross section is given by the summation of $q\bar{q}$ annihilation and Compton processes [52]:

$$\frac{d\sigma^{pA}}{dQ^2 dx_F} = \frac{d\sigma_{q\bar{q}}^{pA}}{dQ^2 dx_F} + \frac{d\sigma_{qg}^{pA}}{dQ^2 dx_F}. \tag{11}$$

They are expressed in terms of the PDFs and subprocess cross sections:

$$\frac{d\sigma_{q\bar{q}}^{pA}}{dQ^2 dx_F} = \frac{4\pi\alpha^2}{9Q^2 s} \sum_i e_i^2 \int_{x_1}^1 dy_1 \int_{x_2}^1 dy_2 \times \left[\frac{d\hat{\sigma}_{q\bar{q}(0)}}{dQ^2 dx_F} + \frac{d\hat{\sigma}_{q\bar{q}(1)}}{dQ^2 dx_F}\right] \left[q_i(y_1, Q^2)\bar{q}_i^A(y_2, Q^2) + \bar{q}_i(y_1, Q^2) q_i^A(y_2, Q^2)\right], \tag{12}$$

$$\frac{d\sigma_{qg}^{pA}}{dQ^2 dx_F} = \frac{4\pi\alpha^2}{9Q^2 s} \sum_i e_i^2 \int_{x_1}^1 dy_1 \int_{x_2}^1 dy_2 \times \left[\frac{d\hat{\sigma}_{gq}}{dQ^2 dx_F} g(y_1, Q^2)\left[q_i^A(y_2, Q^2) + \bar{q}_i^A(y_2, Q^2)\right] + \frac{d\hat{\sigma}_{qg}}{dQ^2 dx_F}\left[q_i(y_1, Q^2) + \bar{q}_i(y_1, Q^2)\right] g^A(y_2, Q^2)\right]. \tag{13}$$

The cross sections $d\hat{\sigma}_{q\bar{q}(0)}$ and $d\hat{\sigma}_{q\bar{q}(1)}$ indicate subprocess cross sections for $q\bar{q}$ annihilation processes in the LO and NLO, respectively. The $d\sigma_{qg}$ indicates the cross section for qg and $\bar{q}g$ processes. The NLO expressions of these cross sections are, for example, found in Ref. [52]. Effects of possible parton-energy loss in the Drell-Yan process [53] are neglected in this analysis.

Using these expressions for the structure functions F_2^A and Drell-Yan cross sections, we calculate the theoretical ratios $R_j^{\rm theo}$ in Eq. (8). The total χ^2 is minimized by the CERN program library MINUIT. From this analysis, an error matrix that is the inverse of a Hessian matrix is obtained. NPDF uncertainties are estimated by using the Hessian matrix as

$$[\delta f^A(x)]^2 = \Delta\chi^2 \sum_{i,j} \left[\frac{\partial f^A(x, \xi)}{\partial \xi_i}\right]_{\xi=\hat{\xi}} H_{ij}^{-1} \left[\frac{\partial f^A(x, \xi)}{\partial \xi_j}\right]_{\xi=\hat{\xi}}, \tag{14}$$

where H_{ij} is the Hessian matrix, ξ_i is a parameter, and $\hat{\xi}$ indicates the optimum parameter set. The $\Delta\chi^2$ value determines the confidence region, and it is calculated so that the confidence level P becomes the one-σ-error range ($P = 0.6826$) for a given number of parameters (N) by assuming the normal distribution in the multiparameter space. In the analysis with the 12 parameters, it is $\Delta\chi^2 = 13.7$. This Hessian method has been used for estimating polarized PDFs and fragmentation functions [54,55] as well as nuclear PDFs in our previous version [18]. The details of the uncertainty analysis are discussed in Refs. [18,54] as well as in the nucleonic PDF articles [56].

III. RESULTS

A. Comparison with data

Determined parameters are listed in Table I for both LO and NLO. Three parameters are fixed by the constraints from baryon-number, charge, and momentum conservations in Eq. (4), and we chose a_{u_v}, a_{d_v}, and a_g for these parameters. The values of the obtained parameters and their errors are similar in the LO and NLO. However, the errors indicate that there are slight NLO improvements in comparison with the LO results.

Each χ^2 contribution is listed in Table II. The values suggest that medium and large nuclei should be well explained by the current LO and NLO parametrizations. However, small nuclei are not so well reproduced. The LO fit (χ^2/DOF = 1.35) is better than the previous analysis with χ^2/DOF = 1.58 [18], which is partly due to the introduction of new parameters for the A dependence in Eq. (6). If the χ^2 values of the LO analysis are compared with the ones in Table III of Ref. [18], we find that much improvements are obtained for the nuclear ratios, $F_2^{\rm Li}/F_2^D$, F_2^C/F_2^D, $F_2^{\rm Be}/F_2^C$, $F_2^{\rm Ca}/F_2^C$, $F_2^{\rm Fe}/F_2^C$, $F_2^{\rm Sn}/F_2^C$, $F_2^{\rm Pb}/F_2^C$, $F_2^{\rm Ca}/F_2^{\rm Li}$, $\sigma_{DY}^{p\rm Ca}/\sigma_{DY}^{pD}$, $\sigma_{DY}^{p\rm Fe}/\sigma_{DY}^{p\rm Be}$, and $\sigma_{DY}^{pW}/\sigma_{DY}^{p\rm Be}$, whereas the fit becomes worse for $\sigma_{DY}^{p\rm Fe}/\sigma_{DY}^{pD}$ and $\sigma_{DY}^{pW}/\sigma_{DY}^{pD}$. The χ^2/DOF is further reduced in the current NLO analysis.

According to Table II, the NLO results with χ^2/DOF = 1.21 reproduce the data better than the LO ones with χ^2/DOF = 1.35, especially in the following data sets: F_2^D/F_2^p, $F_2^{^4\rm He}/F_2^D$, F_2^C/F_2^D, $F_2^{\rm Ca}/F_2^D$, $F_2^{\rm Ag}/F_2^D$, $F_2^{\rm Au}/F_2^D$, $F_2^{\rm Pb}/F_2^D$, $F_2^{\rm Sn}/F_2^C$, $F_2^{\rm Pb}/F_2^C$, and $\sigma_{DY}^{pW}/\sigma_{DY}^{p\rm Be}$, whereas it

TABLE I. Parameters obtained by the LO and NLO analyses. The parameters a_{u_v}, a_{d_v}, and a_g are fixed by the three conservation conditions in Eq. (4). Because they depend on nuclear species, they are explained separately in Appendix A.

Distribution	x_0^+	x_0^-	$d^{(1)}$	$d^{(2)}$	$a^{(1)}$	$a^{(2)}$
(LO)						
u_v^A, d_v^A	0.675 ± 0.005	0.208 ± 0.004	5.089 ± 0.315	0.876 ± 0.143	(Appendix)	(Appendix)
$\bar{q}^A$	0.120 ± 0.007	0.387 ± 0.027	60 (fixed)	0.260 ± 0.043	-0.394 ± 0.027	0.318 ± 0.038
g^A	8.35 ± 9.09	$-x_0^+$ (fixed)	-799 ± 1561	$(0.194 \pm 0.341) \times 10^{-5}$	(Appendix)	(Appendix)
(NLO)						
u_v^A, d_v^A	0.629 ± 0.004	0.178 ± 0.004	6.157 ± 0.254	1.063 ± 0.143	(Appendix)	(Appendix)
$\bar{q}^A$	0.239 ± 0.009	0.119 ± 0.004	150 (fixed)	0.212 ± 0.019	-0.540 ± 0.024	0.295 ± 0.024
g^A	7.24 ± 3.97	$-x_0^+$ (fixed)	-26.5 ± 27.8	$(0.109 \pm 0.114) \times 10^{-3}$	(Appendix)	(Appendix)

TABLE II. Each χ^2 contribution.

Nucleus	Reference	# of data	χ^2 (LO)	χ^2 (NLO)
D/p	[46–49]	290	375.5	322.5
^{4}He/D	[35,38]	35	60.9	51.8
Li/D	[38]	17	36.9	36.4
Be/D	[35]	17	39.3	53.0
C/D	[29,30,35,38,40]	43	105.8	78.7
N/D	[36,41]	162	136.3	121.7
Al/D	[33,35]	35	45.5	44.9
Ca/D	[30,35,38,40]	33	43.3	34.1
Fe/D	[32,34,35,37]	57	108.0	97.4
Cu/D	[31]	19	12.1	13.2
Kr/D	[41]	144	115.1	115.9
Ag/D	[35]	7	12.5	9.1
Sn/D	[29]	8	13.3	14.1
Xe/D	[39]	5	2.2	2.3
Au/D	[34,35]	19	55.6	32.3
Pb/D	[40]	5	5.7	4.5
F_2^A/F_2^D total		606	792.4	709.3
Be/C	[42]	15	12.6	11.9
Al/C	[42]	15	5.0	5.1
Ca/C	[38,42]	39	29.9	29.1
Fe/C	[42]	15	8.0	8.3
Sn/C	[43]	146	204.0	172.1
Pb/C	[42]	15	15.7	12.2
C/Li	[38]	24	67.4	64.9
Ca/Li	[38]	24	69.0	65.3
$F_2^{A_1}/F_2^{A_2}$ total		293	411.6	369.0
C/D	[44]	9	9.3	8.1
Ca/D	[44]	9	5.8	13.8
Fe/D	[44]	9	12.6	17.9
W/D	[44]	9	27.8	29.6
Fe/Be	[45]	8	3.3	3.6
W/Be	[45]	8	14.9	12.1
Drell-Yan total		52	73.8	85.1
Total		1241	1653.3	1485.9
(χ^2/DOF)			(1.35)	(1.21)

becomes worse in F_2^{Be}/F_2^D, $\sigma_{DY}^{p\mathrm{Ca}}/\sigma_{DY}^{pD}$, and $\sigma_{DY}^{p\mathrm{Fe}}/\sigma_{DY}^{pD}$. The deuteron-proton data F_2^D/F_2^p are added in this analysis to the data set of the previous version [18], and they should provide a valuable constraint on PDF modifications in the deuteron. Because the F_2^D/F_2^p data are sensitive to $\bar{u}/\bar{d}$ asymmetry [24], flavor asymmetric antiquark distributions should be used in our analysis. If the flavor symmetric distributions are used as initial ones, the fit produces a significantly larger χ^2.

The fit results of the NLO are compared with the used data in Figs. 1, 2, and 3 for the ratios F_2^A/F_2^D, $F_2^{A_1}/F_2^{A_2}$, and $\sigma_{DY}^{pA_1}/\sigma_{DY}^{pA_2}$, respectively. The rational differences between experimental and theoretical values $(R^{\mathrm{exp}} - R^{\mathrm{theo}})/R^{\mathrm{theo}}$, where R is $R = F_2^A/F_2^D$, $F_2^{A_1}/F_2^{A_2}$, or $\sigma_{DY}^{pA_1}/\sigma_{DY}^{pA_2}$, are shown. For the theoretical values, the NLO results are used and they are calculated at the experimental Q^2 points. The uncertainty bands are also shown in the NLO, and they are calculated at $Q^2 = 10$ GeV^2 for the structure function F_2 and at $Q^2 = 20$ or 50 GeV^2 for the Drell-Yan processes. The scale $Q^2 = 10$ GeV^2 is taken because the average of all the F_2 data is of the order of this value. The scale is $Q^2 = 50$ GeV^2 for the Drell-Yan ratios of the $\sigma_{DY}^{pA}/\sigma_{DY}^{pD}$ type, and the lower scale 20 GeV^2 is taken for the ratio of the $\sigma_{DY}^{pA}/\sigma_{DY}^{p\mathrm{Be}}$ type because experimental Q^2 values are smaller.

These figures indicate that the overall fit is successful in explaining the used data. We notice that the χ^2 values, 53.0, 64.9, and 29.6 in the NLO, are especially large for F_2^{Be}/F_2^D, F_2^C/F_2^{Li}, and $\sigma_{DY}^{pW}/\sigma_{DY}^{pD}$ in comparison with the numbers of their data, 17, 24, and 9, according to Table II. These large χ^2 values come from deviations from accurate E139, NMC, and E772 data; however, such deviations are not very significant in Figs. 1, 2, and 3. There are general tendencies that medium- and large-size nuclei are well explained by our parametrization, whereas there are slight deviations for small nuclei. Because any systematic deviations are not found from the experimental data, our analyses should be successful in determining the optimum nuclear PDFs.

Next, actual data are compared with the LO and NLO theoretical ratios and their uncertainties for the calcium nucleus as an example in Fig. 4. In the upper figures, the theoretical curves and the uncertainties are calculated at fixed Q^2 points,

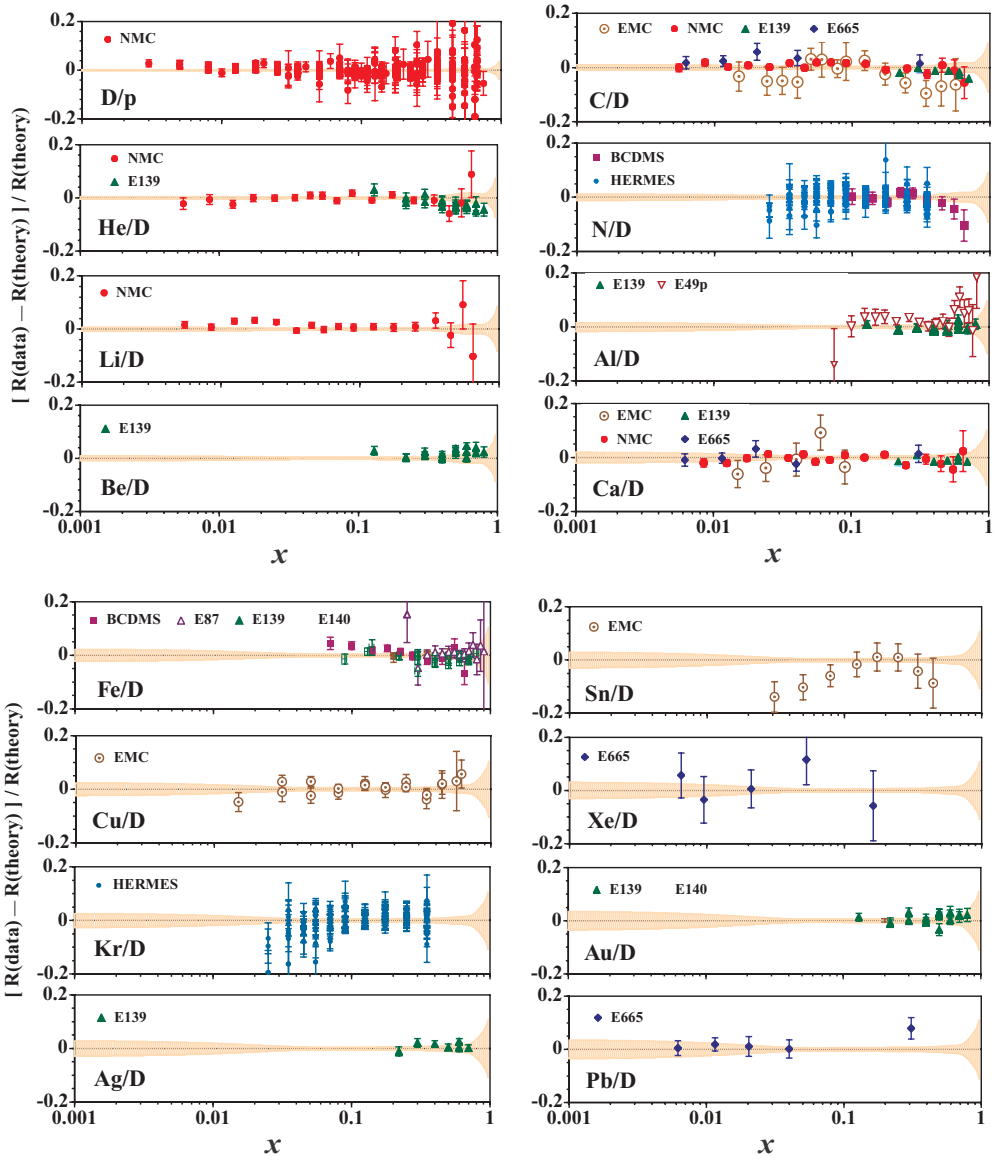

FIG. 1. (Color online) Comparison with experimental ratios $R = F_2^A/F_2^D$ and F_2^D/F_2^p. The rational differences between experimental and theoretical values $[(R^{\rm exp} - R^{\rm theo})/R^{\rm theo}]$ are shown. The NLO parametrization is used for the theoretical calculations at the Q^2 points of the experimental data. Theoretical uncertainties in the NLO are shown at $Q^2 = 10$ GeV^2 by the shaded areas.

$Q^2 = 10$ GeV^2 and 50 GeV^2 for the F_2 and the Drell-Yan, respectively, whereas the experimental data are taken at various Q^2 values. The rational differences $(R^{\rm exp} - R^{\rm theo})/R^{\rm theo}$ are shown together with the difference between the LO and NLO curves, $R^{\rm theo}({\rm LO})/R^{\rm theo}({\rm NLO}) - 1$, in the lower figures. The comparison suggests that both LO and NLO parametrizations should be successful in explaining the x dependence of the calcium data. It is noteworthy that the NLO error band of the F_2 ratio becomes slightly smaller in comparison with the LO one at small x; however, magnitudes of both uncertainties are similar in the region, $x > 0.02$. The NLO improvement is not clearly seen in the Drell-Yan ratio $\sigma_{DY}^{p{\rm Ca}}/\sigma_{DY}^{pD}$ in the range of $x > 0.04$. There are discrepancies between the theoretical curves and the $F_2^{\rm Ca}/F_2^D$ data at $x < 0.01$; however, they are simply due to Q^2 differences. If the theoretical ratios are calculated at the same experimental Q^2 points, they agree as shown in the $F_2^{\rm Ca}/F_2^D$ part of Fig. 1.

These LO and NLO results indicate that the available data are taken in the limited x range without small-x data, and they are not much sensitive to NLO corrections. This fact leads to a difficulty in determining nuclear gluon distributions because the gluonic effects are typical NLO effects through the coefficient functions and in the Q^2 evolution equations.

B. Q^2 dependence

One of possible methods for determining the gluon distribution in the nucleon is to investigate Q^2 dependence of the structure function F_2 [57]. Because Q^2-dependent data

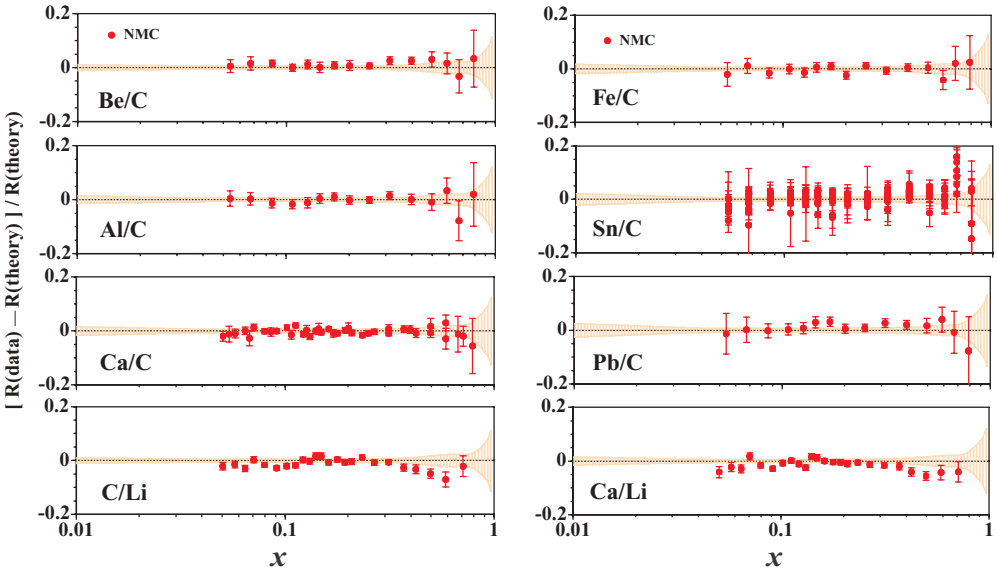

FIG. 2. (Color online) Comparison with experimental data of $R = F_2^A/F_2^{C,\mathrm{Li}}$. The ratios $(R^{\mathrm{exp}} - R^{\mathrm{theo}})/R^{\mathrm{theo}}$ are shown. The theoretical ratios and their uncertainties are calculated in the NLO. The notations are the same as described in the caption to Fig. 1.

exist in the $F_2^A/F_2^{A'}$ ratios, it may be possible to find nuclear modifications of the gluon distribution.

The LO and NLO parametrization results are compared with Q^2-dependent data for F_2^{Kr}/F_2^D and F_2^{Sn}/F_2^C measured by the HERMES and NMC Collaborations, respectively, in Figs. 5 and 6. The uncertainties are shown by the shaded bands in the NLO. Because the LO and NLO uncertainties are similar except for the small-x region, the LO ones are not shown in these figures. They are compared later in this subsection. The results indicate that overall Q^2 dependencies are well explained by our parametrizations in both LO and NLO. The comparison suggests that the experimental data are not accurate enough to probe the details of the Q^2 dependence. Furthermore, Q^2 dependencies of the HERMES and NMC results are different. The HERMES ratio F_2^{Kr}/F_2^D tends to decrease with increasing Q^2 at $x = 0.035$, 0.045, and 0.055, whereas the NMC ratio F_2^{Sn}/F_2^C increases with Q^2 at the same x points, although the nuclear species are different. This kind of difference together with inaccurate Q^2-dependent measurements makes it difficult to extract precise nuclear gluon distributions within the leading-twist DGLAP approach. It is reflected in large uncertainties in the gluon distributions as it becomes obvious in Sec. III C.

In our previous versions [17,18], the experimental shadowing in F_2^{Sn}/F_2^C is underestimated at small x ($0.01 < x < 0.02$) partly because of an assumption on a simple A dependence. As shown in Fig. 6, the shadowing is still slightly underestimated at $x = 0.0125$; however, the deviations are not as large as before. If the experimental errors and the NPDF uncertainties are considered, our parametrization is consistent with the data.

The NLO uncertainties are compared with the LO ones in Fig. 7 for the ratio F_2^{Ca}/F_2^D. The LO and NLO ratios and

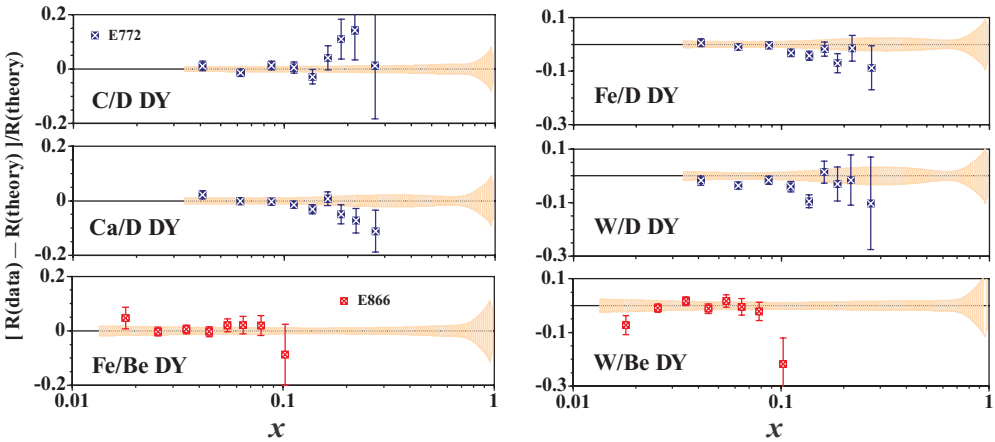

FIG. 3. (Color online) Comparison with Drell-Yan data of $R = \sigma_{DY}^{pA}/\sigma_{DY}^{pA'}$. The ratios $(R^{\mathrm{exp}} - R^{\mathrm{theo}})/R^{\mathrm{theo}}$ are shown. The theoretical ratios and their uncertainties are calculated in the NLO. The theoretical ratios are calculated at the Q^2 points of the experimental data. The uncertainties are estimated at $Q^2 = 20$ and 50 GeV^2 for the the $\sigma_{DY}^{pA}/\sigma_{DY}^{p\mathrm{Be}}$ type and $\sigma_{DY}^{pA}/\sigma_{DY}^{pD}$ one, respectively.

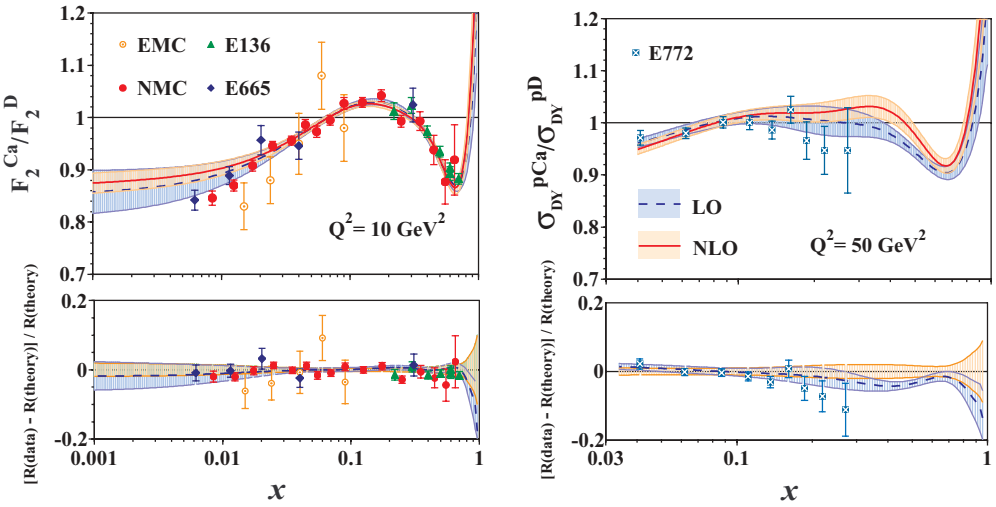

FIG. 4. (Color online) Theoretical results are compared with the data of the F_2 ratio F_2^{Ca}/F_2^D and the Drell-Yan ratio $\sigma_{DY}^{p\mathrm{Ca}}/\sigma_{DY}^{pD}$. In the upper figures, the theoretical curves and uncertainties are calculated at $Q^2 = 10\ \mathrm{GeV}^2$ for the F_2 ratio and at $Q^2 = 50\ \mathrm{GeV}^2$ for the Drell-Yan ratio. The dashed and solid curves indicate LO and NLO results, and the LO and NLO uncertainties are shown by the dark- and light-shaded bands, respectively. The lower figures indicate the ratios $(R^{\mathrm{exp}} - R^{\mathrm{theo}})/R^{\mathrm{theo}}$, where R indicates F_2^{Ca}/F_2^D or $\sigma_{DY}^{p\mathrm{Ca}}/\sigma_{DY}^{pD}$. Here, the theoretical ratios are calculated at the experimental Q^2 points. For comparison, the LO curves and their uncertainties are also shown by $R^{\mathrm{theo}}(\mathrm{LO})/R^{\mathrm{theo}}(\mathrm{NLO}) - 1$ and $\delta R^{\mathrm{theo}}(\mathrm{LO})/R^{\mathrm{theo}}(\mathrm{NLO})$.

their uncertainties are shown at $x = 0.001$, 0.01, 0.1, and 0.7. The differences between both uncertainties are conspicuous at small x ($= 0.001$ and 0.01); however, they are similar at larger x. The LO and NLO slopes are also different at small x. These results indicate that the NLO effects become important at small x (<0.01), and the determination of the NPDFs is improved especially in this small-x region.

Because the NLO contributions are obvious only in the region, $x < 0.01$, it is very important to measure the Q^2 dependence to pin down the NLO effects such as the gluon distributions. The possibilities are measurements at future electron facilities such as eRHIC [58] and eLIC [59].

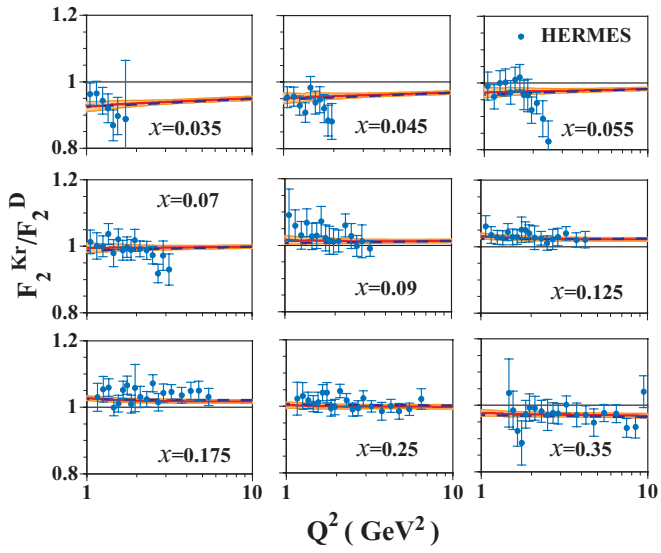

FIG. 5. (Color online) Comparison with Q^2-dependent data of F_2^{Kr}/F_2^D by the HERMES Collaboration. The dashed and solid curves indicate LO and NLO results, and the NLO uncertainties are shown by the shaded bands.

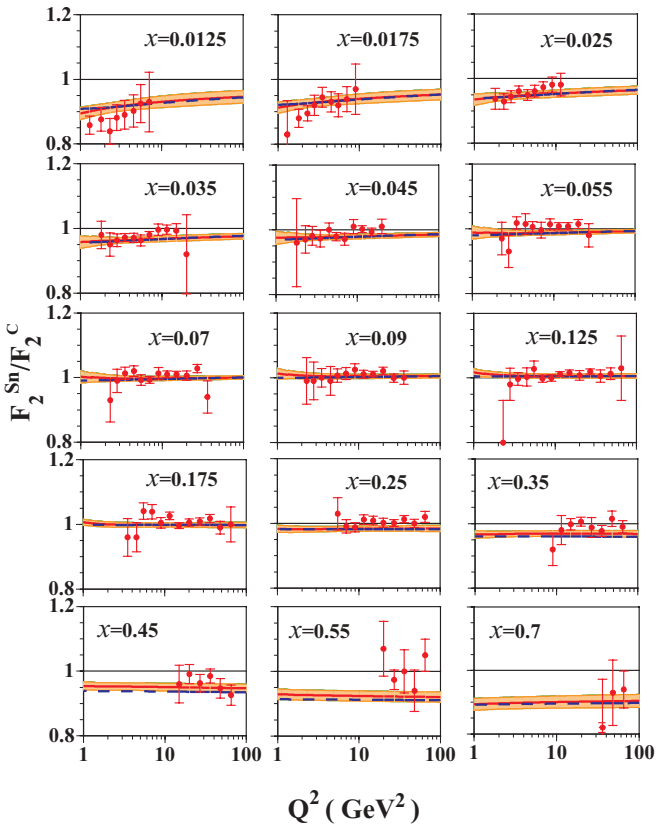

FIG. 6. (Color online) Comparison with Q^2-dependent data of F_2^{Sn}/F_2^C by the NMC. The notations are the same as described in the caption to Fig. 5.

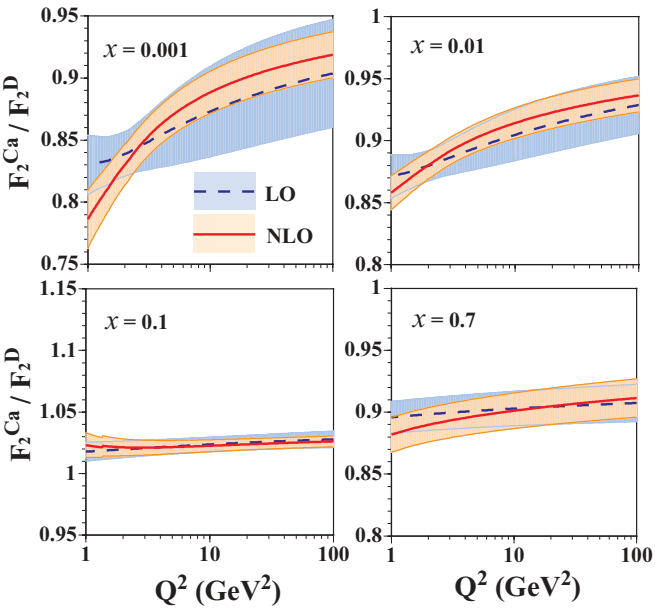

FIG. 7. (Color online) Q^2 dependence of the ratio F_2^{Ca}/F_2^D is compared in the LO and NLO at $x = 0.001$, 0.01, 0.01, and 0.7. The dashed and solid curves indicate LO and NLO results, and LO and NLO uncertainties are shown by the dark- and light-shaded bands, respectively.

C. Parton distribution functions in nuclei

Nuclear modifications of the PDFs are shown for all the analyzed nuclei and ^{16}O at $Q^2 = 1$ GeV^2 in Fig. 8. It should be noted that the modifications of u_v are the same as the ones of d_v in isoscalar nuclei, but they are different in other nuclei. The modifications increase as the nucleus becomes larger, and the dependence is controlled by the overall $1/A^{1/3}$ factor and the A dependence in Eq. (6). The extreme values (x_{0i}^+, x_{0i}^-) are assumed to be independent of A in our current analysis as explained in Sec. II A, so they are the same in Fig. 8. Although the oxygen data are not used in our global analysis, its PDFs are shown in the figure because they are useful for an application to neutrino oscillation experiments [2]. Our code is supplied at the Web site in Ref. [60] for calculating the NPDFs and their uncertainties at given x and Q^2.

As examples of medium and large nuclei, we take the calcium and lead and show their distributions and uncertainties at $Q^2 = 1$ GeV^2 in Fig. 9. Because the deuteron is a special nucleus and it needs detailed explanations, its results are separately discussed in Sec. IV. The figure indicates that valence-quark distributions are determined well in the wide range, $0.001 < x < 1$ because the uncertainties are small. It is also interesting to find that the LO and NLO uncertainties are almost the same. There are following reasons for these results. The valence-quark modifications at $x > 0.3$ are determined by the accurate measurements of F_2 modifications. The antishadowing part in the region $0.1 < x < 0.2$ is also determined by the F_2 data because there is almost no nuclear modification in the antiquark distributions according to the Drell-Yan data. If the valence-quark distributions are obtained at $x > 0.1$, the small-x behavior is automatically constrained by the baryon-number and charge conservations in Eq. (4). Because of these strong constraints, the LO and NLO results are not much different. In the near future, the JLab (Thomas Jefferson National Accelerator Facility) measurements will provide data which could constraint the nuclear valence-quark distribution especially at medium and large x [61]. Furthermore, future neutrino measurements such as the MINERνA experiment at Fermilab [62] and the one at a possible neutrino factory [63] should provide important information at small x ($x =$ 0.01–0.1).

The antiquark distributions are also well determined except for the large-x region, $x > 0.2$, because there is no accurate Drell-Yan data and the structure functions F_2^A are dominated by the valence-quark distributions. The LO and NLO uncertainties are similar except for the large-x region. Because of gluon contributions in the NLO, the antiquark shadowing modifications are slightly different between the LO and NLO. Possible large-x Drell-Yan measurements such as J-PARC (Japan Proton Accelerator Research Complex) [64] and Fermilab-E906 [65] should be valuable for the nuclear antiquark distributions in the whole-x range. In the similar energy region, there is also the GSI-FAIR (Gesellschaft für Schwerionenforschung-Facility for Antiproton and Ion Research) project [66].

The gluon distributions contribute to the F_2 and Drell-Yan ratios as higher-order effects. Therefore, they should be determined more accurately in the NLO analysis than the LO one. Such tendencies are found in Fig. 9 because the NLO uncertainties are smaller than the LO ones in both carbon and lead. However, these NLO improvements are not as clear as the cases of polarized PDF [54] and fragmentation functions [55]. It is because the Q^2-dependent data are not accurate enough to probe such higher-order effects as discussed in Sec. III B. To fix the gluon distributions, accurate measurements are needed for the scaling violation of $F_2^A/F_2^{A'}$ [58,59]. The gluon distributions should be also probed by production processes of such as charged hadrons [67], heavy flavor [68], Υ [69], low-mass dilepton [70], and direct photon [71]. There is a recent study on the gluon shadowing from the HERA diffraction data [72]. Nuclear gluon distributions play an important role in discussing properties of quark-hadron matters in heavy-ion reactions, so they need to be determined experimentally.

We also show the nuclear modifications at $Q^2 =$ 100 GeV^2 for the calcium in Fig. 10. The nuclear modifications are not very different from those at $Q^2 = 1$ GeV^2 for the valence-quark distributions. However, the shadowing corrections become smaller in the antiquark and gluon distributions in comparison with the ones at $Q^2 = 1$ GeV^2, and the modifications tend to increase at medium and large x.

The distribution functions themselves and their uncertainties are shown in Figs. 11 and 12 for the calcium and lead, respectively. Both LO and NLO distributions are shown. Here, the uncertainties from the nucleonic PDFs are not included in the uncertainty bands. The calcium is an isoscalar nucleus, so u_v^A and $\bar{u}^A$ are equal to d_v^A and $\bar{d}^A$. However, they are different in the lead nucleus because of the neutron excess. To see nuclear modification effects, we show the distributions without the nuclear modifications. For example, the distribution $(\mathrm{Z}u_v + \mathrm{N}d_v)/A$ is shown in the figure of u_v^A by using the MRST distributions for u_v and d_v. Although the

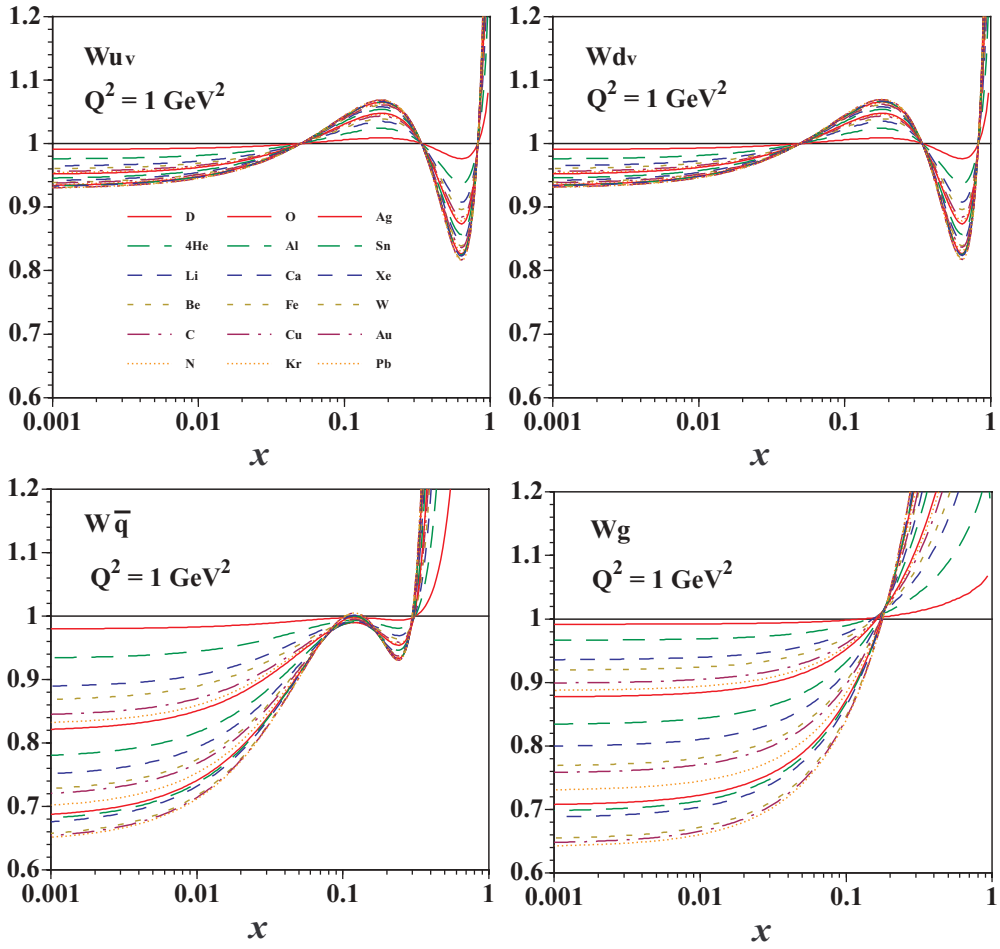

FIG. 8. (Color online) Nuclear modifications w_i ($i = u_v, d_v, \bar{q}$, and g) are shown in the NLO for all the analyzed nuclei and ^{16}O at $Q^2 = 1$ GeV^2. As the mass number becomes larger in the order of D, ^{4}He, Li,. . ., and Pb, the curves deviate from the line of unity ($w_i = 1$).

uncertainties are large in the antiquark and gluon distributions at medium and large x, they are not very conspicuous in Figs. 11 and 12 because the distributions themselves are small.

The flavor asymmetric antiquark distributions are assumed in this analysis as they are defined in Eq. (2). From this definition, it is obvious that $\bar{u}^A$ and $\bar{d}^A$ are equal in isoscalar nuclei such as carbon and calcium. In Fig. 13, the ratio $(\bar{u}^A - \bar{d}^A)/(u^A - d^A)$ is shown for the proton (p), lithium (Li), aluminum (Al), iron (Fe), and lead (Pb) at $Q^2 = 1$ GeV^2. Because the nuclear corrections are assumed to be equal for the antiquark distributions at Q_0^2 in Eq. (2), they are almost independent of nuclear species except for the isoscalar nuclei. It is interesting to investigate possible nuclear modifications on the distribution $\bar{u} - \bar{d}$ at the future facilities [64,65].

There are noticeable differences between our NLO analysis results and the ones in Ref. [19], especially in the strange-quark and gluon modifications. These differences come from various sources. First, the analyzed experimental data sets are slightly different. Second, the strange-quark distributions are created by the DGLAP evolution by assuming $s(x) = 0$ at the initial Q^2 scale, and the charm distributions are neglected in Ref. [19]. These differences lead to the discrepancies of the gluon modifications.

The determined NPDFs and their uncertainties can be calculated by using our code, which is supplied on our Web site [60]. By providing a kinematical condition for x and Q^2 and also a nuclear species, one can calculate the NPDFs. It is explained in Appendix B. If one needs analytical expressions of the NPDFs at the initial scale Q_0^2, one may read instructions in Appendix A.

IV. NUCLEAR MODIFICATIONS IN DEUTERON

Nuclear densities are usually independent of the mass number, which indicates that the average nucleon separation is constant in nuclei. However, the deuteron is a special nucleus in the sense that its radius is about 4 fm, which is much larger than the average nucleon separation in ordinary nuclei ($\sim$2 fm). Because it is a dilute system, nuclear modifications are often neglected. In fact, corrections to nucleonic structure functions and PDFs are small, namely within a few percentages according to theoretical estimates [73–77] even if they are taken into account.

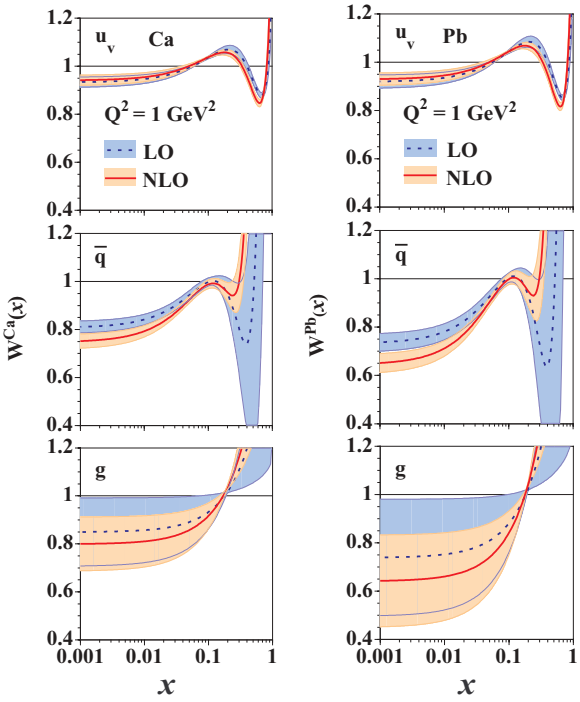

FIG. 9. (Color online) Nuclear modifications of the PDFs and their uncertainties are shown for the calcium and lead nuclei at $Q^2 = 1$ GeV^2. The dashed and solid curves indicate LO and NLO results, and LO and NLO uncertainties are shown by the dark- and light-shaded bands, respectively.

Theoretical modifications in the deuteron depend much on models. The shadowing of Ref. [73], which was used in the MRST analysis, is 1.1% at $x = 0.015$ and $Q^2 = 4$ GeV^2; however, other model calculations are different, 0.5−3.5% at $x \sim 0.01$ as shown in Table III. Furthermore, the modifications at medium x could be as large as or larger than the small-x shadowing (for example, 5% at $x = 0.6$–0.7 according to Ref. [76]).

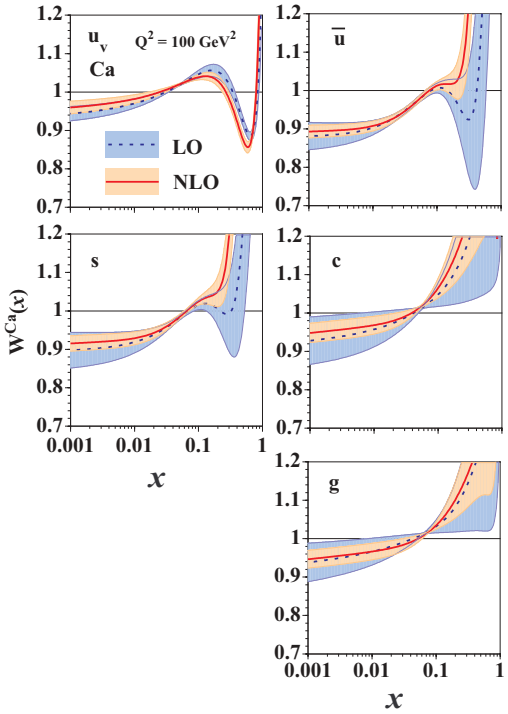

FIG. 10. (Color online) Nuclear modifications are shown for the calcium at $Q^2 = 100$ GeV^2.

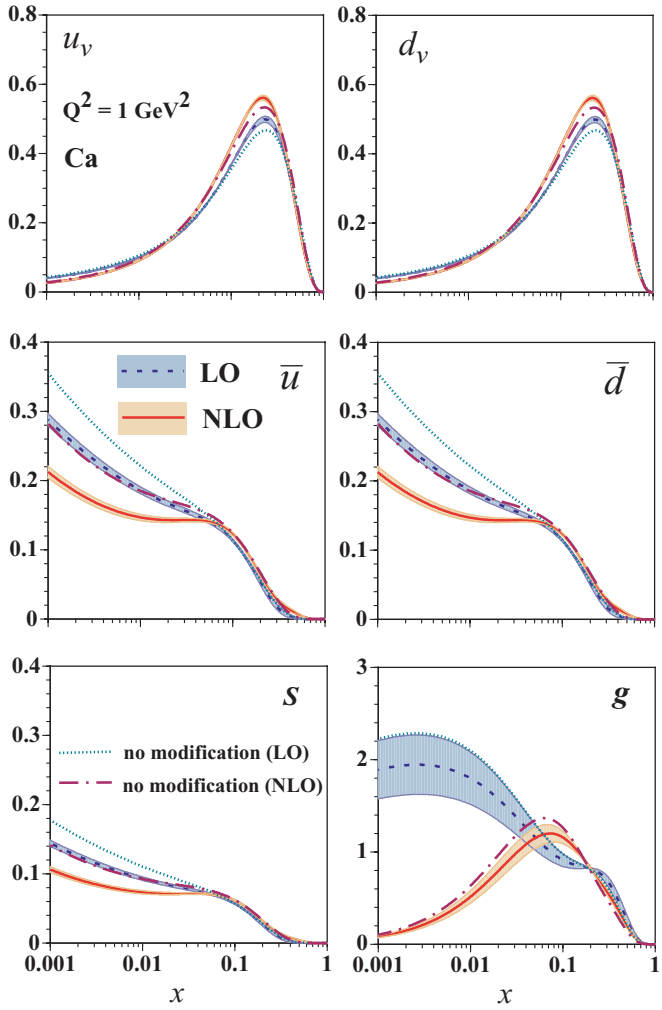

FIG. 11. (Color online) Parton distribution functions in the calcium at $Q^2 = 1$ GeV^2. "No modification" indicates, for example, the distribution $(\mathrm{Zu}_v + \mathrm{Nd}_v)/A$ in the figure of u_v^A.

Such deuteron corrections are becoming important recently although the magnitude itself may not be large. For example, precise nuclear modifications need to be taken into account

TABLE III. Theoretical model estimations for nuclear modification of F_2 in the deuteron at $x \sim 0.01$.

Reference	Q^2 (GeV^2)	x	Modification (%)
[73]	4	0.015	1.1
[74]	4	0.010	2.5
[75]	4	0.010	2.0
[76]	4	0.010	0.4−0.8
[77]	4	0.010	1−2 (3.5)

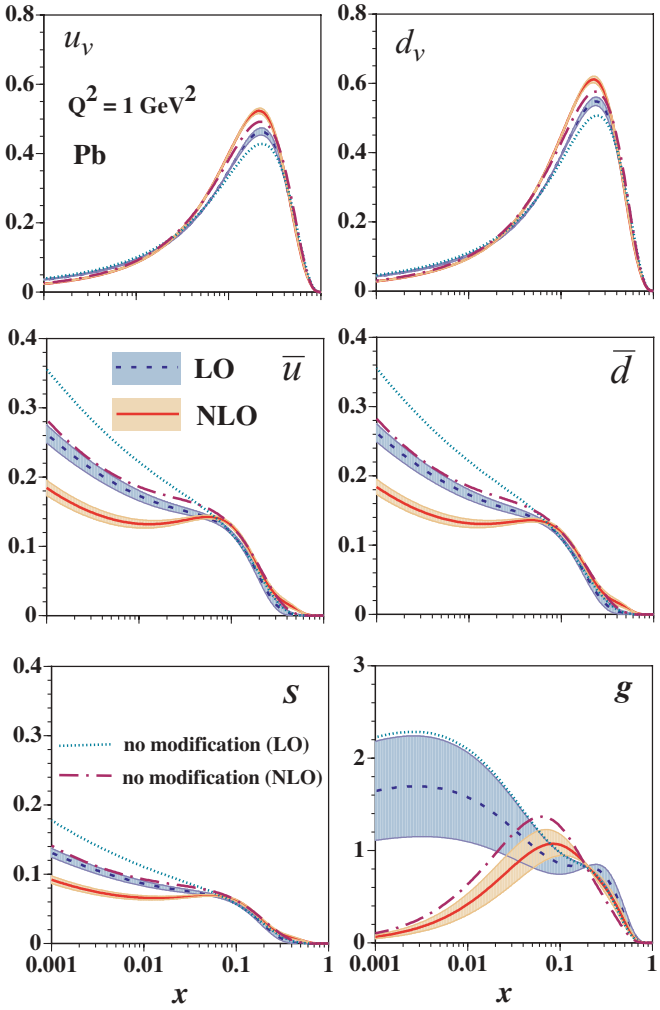

FIG. 12. (Color online) Parton distribution functions in the lead at $Q^2 = 1$ GeV^2. "No modification" indicates, for example, the distribution $(\mathrm{Zu}_v + \mathrm{Nd}_v)/A$ in the figure of u_v^A.

for investigating quark-hadron matters in heavy-ion collisions such as deuteron-gold reactions in comparison with deuteron-

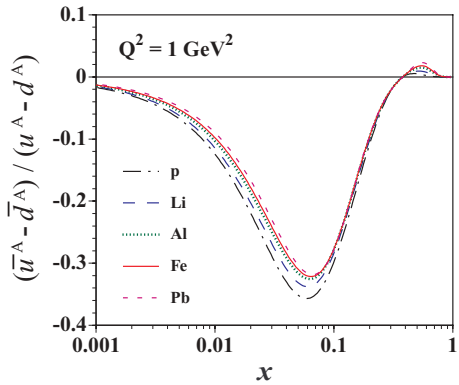

FIG. 13. (Color online) The ratio of flavor asymmetric distributions, $(\bar{u}^A - \bar{d}^A)/(u^A - d^A)$, is shown for the proton, lithium, aluminum, iron, and lead at $Q^2 = 1$ GeV^2. In the isoscalar nuclei, the distributions vanish $(\bar{u}^A - \bar{d}^A = 0)$.

deuteron ones at RHIC [1]. They are also valuable for discussing Gottfried-sum-rule violation and flavor-asymmetric antiquark distributions because deuteron targets are used [24].

In our previous versions on the NPDFs [17,18], the data of F_2^D/F_2^p are not included in the used data set. Obtained nuclear modifications tend to be large in comparison with the theoretical model estimations. For example, the HKN04 analysis [18,60] indicates about 6 and 8% corrections in antiquark and gluon distributions, respectively, at small x ($\sim$0.01) with $Q^2 = 1$ GeV^2 and about 5% in valence-quark ones at medium x ($\sim$0.7). They are possibly overestimations in the sense that typical theoretical models have corrections within the order of a few percentages.

To obtain reasonable deuteron modifications from experimental data, we added F_2^D/F_2^p measurements into the data set in our χ^2 analysis. These deuteron data were already included in the analysis results in Sec. III. In addition to the analysis of Sec. III, two other analyses have been made by modifying Eq. (3):

$$w_i(x, A, Z) = 1 + e_d \left(1 - \frac{1}{A^\alpha}\right) \frac{a_i + b_i x + c_i x^2 + d_i x^3}{(1-x)^{\beta_i}}. \tag{15}$$

An additional factor e_d is introduced. The analysis results in Sec. III correspond to the $e_d = 1$ case. The other analyses have been made by taking $e_d = 0$ and by taking it as a free parameter. We call them analyses 1, 2, and 3, respectively:

(i) analysis 1: $e_d = 1$,
(ii) analysis 2: $e_d = 0$,
(iii) analysis 3: $e_d =$ free parameter.

The χ^2 values of these analyses are listed in Table IV.

The deuteron modifications are terminated in the analysis 2 by taking $e_d = 0$. Although such an assumption does not seem to make sense, we found a smaller χ^2 value from the F_2^D/F_2^p data than the one of the first analysis as shown in Table IV. There are three major reasons for this result. First, the deuteron modifications obtained by the overall A dependence in Eq. (3) are too large because the deuteron is a loosely bound system that is much different from other nuclei. Smaller modifications are expected from the large nucleon separation. Second, deuteron data are used for determining the PDFs in the "nucleon" [26] by considering nuclear shadowing modifications of Ref. [73]. The modifications are calculated in a vector-meson-dominance mechanism and the shadowing in the deuteron is about 1% at $x \sim 0.01$ according to this model. If this shadowing is not a realistic correction, the

TABLE IV. Each χ^2 contribution.

Nucleus	# of data	χ^2 ($e_d = 1$)	χ^2 ($e_d = 0$)	χ^2 (free)
D/p	290	322.5	282.6	284.9
F_2^A/F_2^D	606	709.3	704.8	703.8
$F_2^{A_1}/F_2^{A_2}$	293	369.0	381.6	375.3
Drell-Yan	52	85.1	84.5	85.4
Total	1241	1485.9	1453.4	1449.4
(χ^2/DOF)		(1.21)	(1.18)	(1.18)

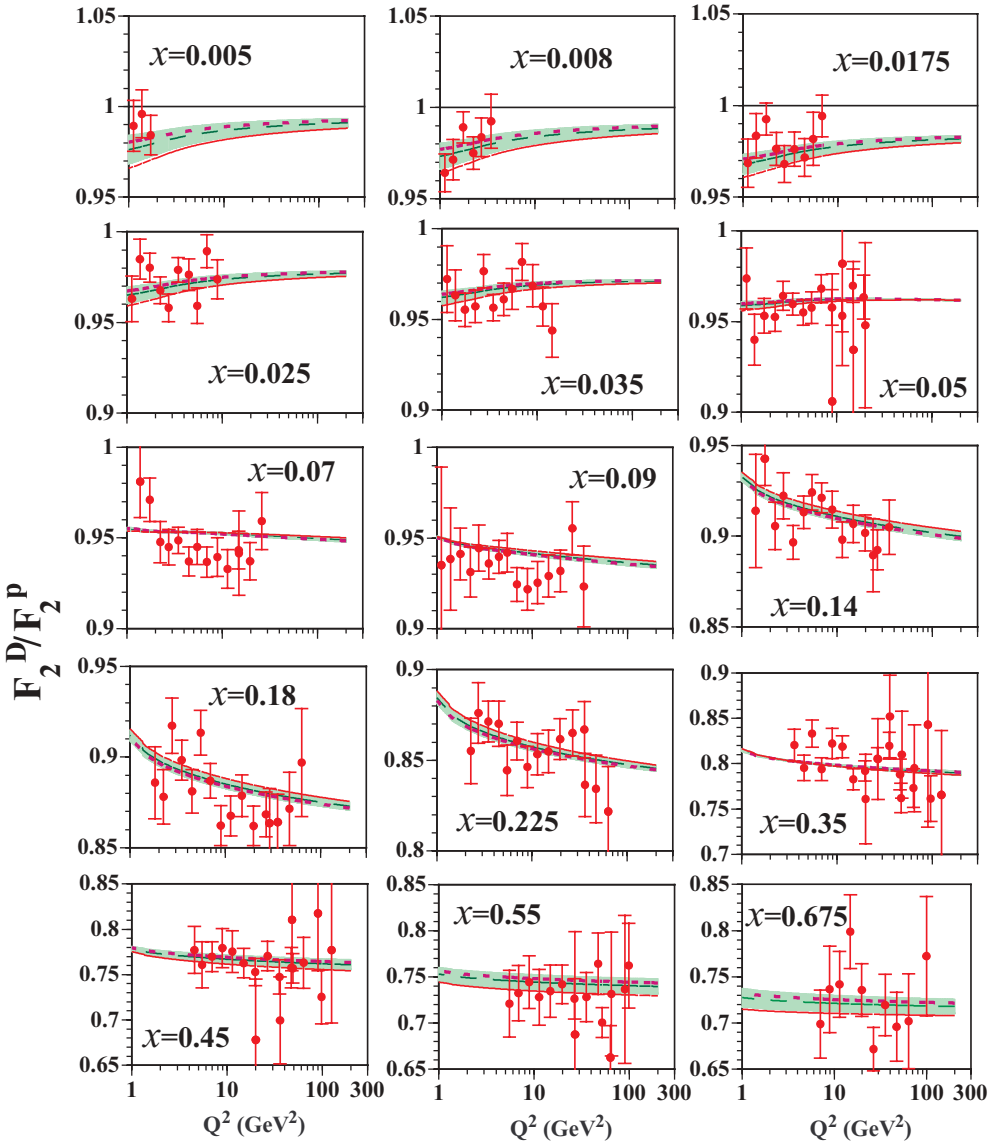

FIG. 14. (Color online) Comparison with the NMC data of F_2^D/F_2^p. The solid, dotted, and dashed curves indicate the NLO results of the analyses 1 ($e_d = 1$), 2 ($e_d = 0$), and 3 ($e_d =$ free), respectively. The shaded bands indicate uncertainties of the analysis-3 curves.

nucleonic PDFs of the MRST should partially contain nuclear effects at small x. The medium- and large-x regions are not corrected, so some deuteron effects could be also included in the nucleonic PDFs in these regions. However, the corrections are not experimentally obvious in such x regions as we find in the actual data of Fig. 14. In this way, the nucleonic PDFs could contain some deuteron modification effects. Third, the nuclear effects could be absorbed into the $\bar{u}/\bar{d}$ asymmetry because it is determined partially by the F_2^D/F_2^p data. These are the possible reasons why analysis 2 produces the smaller χ^2 value.

In the third analysis, the additional parameter e_d is determined from the global analysis. As mentioned, the internucleon separation is exceptionally large in the deuteron. It leads to small nuclear corrections, which are much smaller than a smooth A-dependent functional form, as calculated in various models [73–77] in Table III. These models could be used for estimating an appropriate value for e_d. However, we try to determine the nuclear PDFs without relying on specific theoretical models. The modification parameter e_d is determined from the experimental data, and our analysis 3 indicates $e_d = 0.304 \pm 0.141$. If the diffuse deuteron system is considered, the 70% reduction may make sense. Nonetheless, it should be noted that this factor may not reflect a realistic modification because it is likely that the deuteron effects are contained in the nucleonic PDFs.

We show actual comparisons with the experimental data for F_2^D/F_2^p by the NMC in Fig. 14. Three global analysis results are shown, and the shaded areas indicate uncertainty bands in analysis 3. The figure suggests that all the analyses are successful in explaining the data. However, as indicated in the χ^2 reductions in the analyses 2 and 3, it is clear that their curves are closer to the experimental data at small x such as $x = 0.005$ and 0.008. There is a tendency that deviations

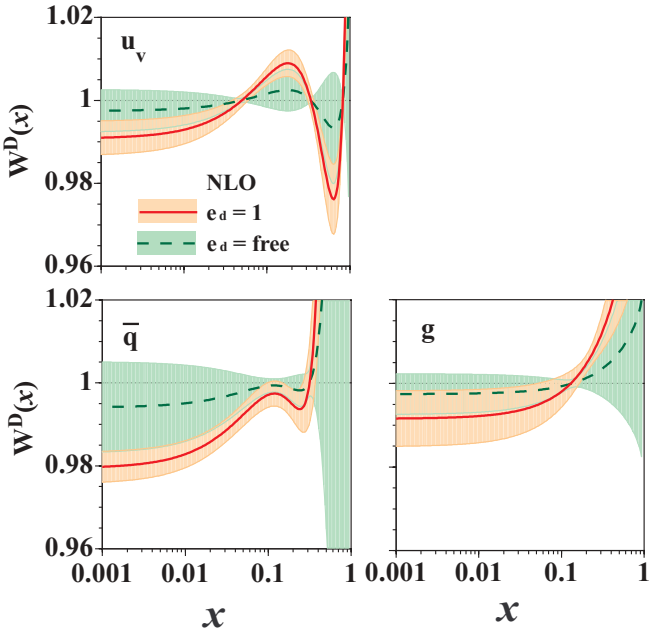

FIG. 15. (Color online) Nuclear modifications of the PDFs and their uncertainties are shown for the deuteron at $Q^2 = 1$ GeV^2. The solid and dashed curves are obtained by analyses 1 and 3, respectively, and their uncertainties are shown by the shaded bands.

from the data become larger as the deuteron modifications are increased. All the analysis results are more or less similar in the medium- and large-x regions. All the curves of the analysis 1 ($e_d = 1$) and 2 ($e_d = 0$) are within the uncertainty bands of the analysis 3 ($e_d =$ free), although the analysis-1 curves are at the edges of the error bands at small x. It means that all these analysis are consistent with each other and they explain the experimental data.

Modifications of the PDFs are shown for the deuteron in Fig. 15 at $Q^2 = 1$ GeV^2. The results of analyses 1 and 3 are shown with their uncertainty estimation. There is no deuteron modification in analysis 2 as obvious from the definition in Eq. (15). The uncertainty bands of analysis 3 shrink at the points, where the nuclear modifications vanish ($w^D = 1$), for example, in the figure of the valence-quark modification w_{u_v}. This is caused by the error from the parameter e_d. Its contributions to the uncertainties are large and the derivative $\partial w_{u_v}/\partial e_d$ is proportional to $a_{u_v} + b_v x + c_v x^2 + d_v x^3$, which vanishes at the same points as the function $w^D_{u_v}(x) - 1 = 0$ in Eq. (15). It leads to the gourd-shaped uncertainty band in w_{u_v} because other terms are small. Such an error shape does not appear in analysis 1 because the error term of e_d does not exist. Here, the derivative $\partial w_{u_v}/\partial d_v^{(1)}$ is also a cubic polynomial and vanishes at three x points. However, $\partial w_{u_v}/\partial x_{0v}^+$ and $\partial w_{u_v}/\partial x_{0v}^-$ are quadratic functions, which do not vanish at the same x points, and their contributions to the uncertainties are of the same order of the $d_v^{(1)}$ and $d_v^{(2)}$ terms. This is the reason why such a gourd-shaped function does not appear in the uncertainties of the $e_d = 1$ analysis.

The antiquark shadowing is about 2% at $x = 0.01$ and the valence-quark modification is about 1% in the analysis 1 according to Fig. 15. We should note that the antiquark shadowing is reduced about 30% at $Q^2 = 4$ GeV^2 as shown in Fig. 7 in comparing it with the theoretical values in Table III. In analysis 3, the antiquark shadowing becomes 0.5%, which could be slightly smaller than the theoretical ones. Both corrections (2 and 0.5%) are slightly different from the assumed correction (1% at $x = 0.01$ and $Q^2 = 4$ GeV^2) in the MRST fit. The uncertainty bands depend on the initial functional form or assignment of the parameters in the χ^2 analysis. The uncertainties are generally larger in analysis 3, and the line of $w^D = 1$ is within the bands. It suggests that precise deuteron modifications cannot be determined at this stage. The modifications in Fig. 15 may not be seriously taken because the deuteron effects could be partially included in the nucleonic PDFs. It is difficult to judge what the realistic deuteron modifications are at this stage. Actual modifications are possibly in between these analysis results.

To obtain realistic modifications, the nucleonic PDFs should be determined by considering the deuteron modifications, for example, of our analysis results. Then, using new nucleonic PDFs, we redetermine our nuclear PDFs including the ones in the deuteron. Realistic deuteron modifications should be obtained by repeating this step.

V. SUMMARY

Nuclear PDFs have been determined by the global analyses of experimental data for the ratios of the F_2 structure functions and Drell-Yan cross sections. The uncertainties of the determined NPDFs are estimated by the Hessian method. The first important point is that the uncertainties were obtained in both LO and NLO so we can discuss the NLO improvement on the determination. We found slight NLO improvements for the antiquark and gluon distributions at small x ($\sim$0.001); however, they are not significant at larger x. Accurate experimental measurements, especially on the Q^2 dependence at small x, should be useful for determining higher-order effects such as the nuclear gluon distributions.

The valence-quark distributions are well determined. The antiquark distributions are also determined at $x < 0.1$; however, they have large uncertainties at $x > 0.2$. The gluon modifications are not precisely determined in the whole x region. Future measurements are needed to determine accurate nuclear distributions.

Nuclear modifications were discussed for the deuteron in comparison with the experimental data of F_2^D/F_2^p. However, it is difficult to find accurate modifications at this stage because deuteron effects could be partially contained in the nucleonic PDFs. An appropriate nucleonic PDF analysis is needed in addition to accurate measurements on the ratio F_2^D/F_2^p.

Our NPDFs and their uncertainties can be calculated by using the codes in Ref. [60].

ACKNOWLEDGMENTS

M.H. and S.K. were supported by the Grant-in-Aid for Scientific Research from the Japanese Ministry of Education, Culture, Sports, Science, and Technology. T.-H.N. was supported by Japan Society for the Promotion of Science.

APPENDIX A: PARAMETERS a_{u_v}, a_{d_v}, AND a_g

The determined parameters are listed in Table I. There are other parameters, a_{u_v}, a_{d_v}, and a_g, that are automatically calculated from the tabulated values by the conservation conditions of nuclear charge, baryon number, and momentum in Eq. (4). Because they depend on nuclear species, namely on A and Z, their calculation method is explained in the following. The flavor asymmetric antiquark distributions in Eq. (2) are used in this analysis, whereas the flavor symmetric ones are used in the previous versions in Refs. [17,18], so relations are slightly different from the ones in Appendix of Ref. [17]. One can obtain values of these parameters for any nuclei by calculating the following integrals:

$$\begin{aligned}
I_1(A) &= \int dx \frac{H_v(x,A)}{(1-x)^{\beta_v}} u_v(x), \\
I_2(A) &= \int dx \frac{H_v(x,A)}{(1-x)^{\beta_v}} d_v(x), \\
I_3 &= \int dx \frac{1}{(1-x)^{\beta_v}} u_v(x), \\
I_4 &= \int dx \frac{1}{(1-x)^{\beta_v}} d_v(x), \\
I_5 &= \int dx \frac{x}{(1-x)^{\beta_v}} u_v(x), \\
I_6 &= \int dx \frac{x}{(1-x)^{\beta_v}} d_v(x), \\
I_7(A) &= \int dx x \left\{ \frac{H_v(x,A)}{(1-x)^{\beta_v}} [u_v(x) + d_v(x)] \right. \\
&\quad + \frac{a_{\bar{q}}(A) + H_{\bar{q}}(x,A)}{(1-x)^{\beta_{\bar{q}}}} 2[\bar{u}(x) + \bar{d}(x) \\
&\quad \left. + \bar{s}(x)] + \frac{H_g(x,A)}{(1-x)^{\beta_g}} g(x) \right\}, \\
I_8 &= \int dx \frac{x}{(1-x)^{\beta_g}} g(x),
\end{aligned} \tag{A1}$$

where $\beta_v = \beta_{\bar{q}} = \beta_g = 0.1$ and $H_i(x, A)$ is

$$H_i(x, A) = b_i x + c_i x^2 + d_i(A) x^3. \tag{A2}$$

Here, the parameters d_v, $a_{\bar{q}}$, $d_{\bar{q}}$, and d_g depend on A according to Eq. (6). It is noteworthy that the integrals I_1, I_2, and I_7 depend on A. Using these integrals, one obtains parameter values by the conservations in Eq. (4):

$$a_{u_v}(A, Z) = -\frac{Z I_1(A) + (A - Z) I_2(A)}{Z I_3 + (A - Z) I_4}, \tag{A3}$$

$$a_{d_v}(A, Z) = -\frac{Z I_2(A) + (A - Z) I_1(A)}{Z I_4 + (A - Z) I_3}, \tag{A4}$$

$$\begin{aligned}
a_g(A, Z) = -\frac{1}{I_8} \Bigg\{ & a_{u_v}(A, Z) \left[\frac{Z}{A} I_5 + \left(1 - \frac{Z}{A}\right) I_6 \right] \\
& + a_{d_v}(A, Z) \left[\frac{Z}{A} I_6 + \left(1 - \frac{Z}{A}\right) I_5 \right] + I_7(A) \Bigg\}.
\end{aligned} \tag{A5}$$

From these values together with the parameters in Table I and the nucleonic PDFs at $Q^2 = 1$ GeV^2 of the MRST parametrization [26], one obtains the NPDFs at $Q^2 = 1$ GeV^2 for a given nucleus. If distributions are needed at different Q^2, one needs to evolve the NPDFs by using own evolution code. If one does not have such an evolution code, one had better use the code in Appendix B. Numerical values of the NPDFs can be obtained for given x, Q^2, and A. In particular, if one is interested in estimating the uncertainties of the NPDFs, this practical code needs to be used.

APPENDIX B: CODE FOR CALCULATING NUCLEAR PARTON DISTRIBUTION FUNCTIONS AND THEIR UNCERTAINTIES

Codes for calculating nuclear PDFs and their uncertainties can be obtained from the Web site [60]. A general guideline for usage is explained in Appendix B of Ref. [18], and the conditions are the same in the current version, HKN07 (Hirai, Kumano, Nagai in 2007). Therefore, the details should be found in Ref. [18]. The NPDFs can be calculated for nuclei at given x and Q^2, for which the kinematical ranges should be in $10^{-9} \leqslant x \leqslant 1$ and 1 GeV$^2 \leqslant Q^2 \leqslant 10^8$ GeV^2.

Input parameters for running the code are explained in the beginning of the file npdf07.f. A sample program, sample.f, is supplied as an example for calculating the nuclear PDFs and uncertainties. The uncertainties of the NPDFs are estimated by using the Hessian matrix and grid data for derivatives with respect to the parameters. The usage is explained in the sample program.

[1] J. Adams *et al.*, Phys. Rev. Lett. **97**, 152302 (2006); B. A. Cole *et al.*, hep-ph/0702101; L. C. Bland *et al.*, Eur. Phys. J. C **43**, 427 (2005); V. Guzey, M. Strikman, and W. Vogelsang, Phys. Lett. **B603**, 173 (2004); P. Jacobs and X.-N. Wang, Prog. Part. Nucl. Phys. **54**, 443 (2005).

[2] M. Sakuda, Nucl. Phys. **B112**, 109 (2002); E. A. Paschos and J. Y. Yu, Phys. Rev. D **65**, 033002 (2002).

[3] J. Jalilian-Marian and Y. V. Kovchegov, Prog. Part. Nucl. Phys. **56**, 104 (2006); E. Iancu and R. Venugopalan, in *Quark Gluon Plasma 3*, edited by R. C. Hwa and X. N. Wang (World Scientific, Singapore, 2003).

[4] F. Arleo and V.-N. Tram, hep-ph/0612043.

[5] T. Renk and J. Ruppert, Phys. Rev. C **72**, 044901 (2005); Phys. Lett. **B646**, 19 (2007).

[6] A. Accardi *et al.*, hep-ph/0308248, in Hard Probes in Heavy Ion Collisions at the LHC, CERN Yellow Reports, CERN-2004-009 (2004), edited by M. L. Mangano, H. Satz, and U. A. Wiedemann (2004).

[7] A. Bodek and U. K. Yang, Nucl. Phys. **B112**, 70 (2002); For summary, see W. Melnitchouk, R. Ent, and C. Keppel, Phys. Rep. **406**, 127 (2005).

[8] G. P. Zeller *et al*., Phys. Rev. Lett. **88**, 091802 (2002); Erratum, *ibid*. **90**, 239902 (2003).
[9] S. Kumano, Phys. Rev. D **66**, 111301(R) (2002); M. Hirai, S. Kumano, and T.-H. Nagai, *ibid*. **71**, 113007 (2005).
[10] S. J. Brodsky, I. Schmidt, and J.-J. Yang, Phys. Rev. D **70**, 116003 (2004).
[11] K. J. Eskola and H. Paukkunen, JHEP 06 (2006) 008.
[12] J. F. Owens *et al*., Phys. Rev. D **75**, 054030 (2007); After submitting this paper for publication, we noticed the work on nuclear PDFs in the iron, I. Schienbein *et al*., arXiv:0710.4897v1 [hep-ph].
[13] For summary, see D. F. Geesaman, K. Saito, and A. W. Thomas, Annu. Rev. Nucl. Part. Sci. **45**, 337 (1995); N. Armesto, J. Phys. G **32**, R367 (2006).
[14] C. J. Benesh, T. Goldman, and G. J. Stephenson, Phys. Rev. C **68**, 045208 (2003); H. Mineo *et al*., Nucl. Phys. **A735**, 482 (2004); I. C. Cloet, W. Bentz, and A. W. Thomas, Phys. Rev. Lett. **95**, 052302 (2005); Phys. Lett. **B642**, 210 (2006); G. A. Miller, Eur. Phys. J. A **31**, 578 (2007).
[15] http://durpdg.dur.ac.uk/HEPDATA/.
[16] K. J. Eskola *et al*., Nucl. Phys. **B535**, 351 (1998); Eur. Phys. J. C **9**, 61 (1999); JHEP 05 (2007) 002.
[17] M. Hirai, S. Kumano, and M. Miyama, Phys. Rev. D **64**, 034003 (2001).
[18] M. Hirai, S. Kumano, and T.-H. Nagai, Phys. Rev. C **70**, 044905 (2004).
[19] D. de Florian and R. Sassot, Phys. Rev. D **69**, 074028 (2004).
[20] N. Armesto, Eur. Phys. J. C **26**, 35 (2002); N. Armesto *et al*., *ibid*. **29**, 531 (2003).
[21] J. Qiu and I. Vitev, Phys. Rev. Lett. **93**, 262301 (2004).
[22] L. Frankfurt, V. Guzey, and M. Strikman, Phys. Rev. D **71**, 054001 (2005).
[23] S. A. Kulagin and R. Petti, Nucl. Phys. **A765**, 126 (2006).
[24] S. Kumano, Phys. Rep. **303**, 183 (1998); G. T. Garvey and J.-C. Peng, Prog. Part. Nucl. Phys. **47**, 203 (2001).
[25] H.-L. Lai *et al*., JHEP 04 (2007) 089; D. Mason, Proceedings of the 14th International Workshop on Deep Inelastic Scattering (World Scientific, Singapore, 2007), pp. 165–168.
[26] A. D. Martin, R. G. Roberts, W. J. Stirling, and R. S. Thorne, Eur. Phys. J. C **4**, 463 (1998).
[27] I. Sick and D. Day, Phys. Lett. **B274**, 16 (1992).
[28] L. L. Frankfurt, M. I. Strikman, and S. Liuti, Phys. Rev. Lett. **65**, 1725 (1990).
[29] J. Ashman *et al*., Phys. Lett. **B202**, 603 (1988).
[30] M. Arneodo *et al*., Nucl. Phys. **B333**, 1 (1990).
[31] J. Ashman *et al*., Z. Phys. C **57**, 211 (1993).
[32] A. Bodek *et al*., Phys. Rev. Lett. **50**, 1431 (1983).
[33] A. Bodek *et al*., Phys. Rev. Lett. **51**, 534 (1983).
[34] S. Dasu *et al*., Phys. Rev. Lett. **60**, 2591 (1988).
[35] J. Gomez *et al*., Phys. Rev. D **49**, 4348 (1994).
[36] G. Bari *et al*., Phys. Lett. **B163**, 282 (1985).
[37] A. C. Benvenuti *et al*., Phys. Lett. **B189**, 483 (1987).
[38] P. Amaudruz *et al*., Nucl. Phys. **B441**, 3 (1995); M. Arneodo *et al*., *ibid*. **B441**, 12 (1995).
[39] M. R. Adams *et al*., Phys. Rev. Lett. **68**, 3266 (1992).
[40] M. R. Adams *et al*., Z. Phys. C **67**, 403 (1995).
[41] A. Airapetian *et al*., Phys. Lett. **B475**, 386 (2000); Erratum, *ibid*. **B567**, 339 (2003).
[42] M. Arneodo *et al*., Nucl. Phys. **B481**, 3 (1996).
[43] M. Arneodo *et al*., Nucl. Phys. **B481**, 23 (1996).
[44] D. M. Alde *et al*., Phys. Rev. Lett. **64**, 2479 (1990).
[45] M. A. Vasiliev *et al*., Phys. Rev. Lett. **83**, 2304 (1999).
[46] J. J. Aubert *et al*., Nucl. Phys. **B293**, 740 (1987).
[47] A. C. Benvenuti *et al*., Phys. Lett. **B237**, 599 (1990).
[48] M. R. Adams *et al*., Phys. Rev. Lett. **75**, 1466 (1995).
[49] M. Arneodo *et al*., Nucl. Phys. **B487**, 3 (1997).
[50] M. Miyama and S. Kumano, Comput. Phys. Commun. **94**, 185 (1996); M. Hirai, S. Kumano, and M. Miyama, *ibid*. **108**, 38 (1998); **111**, 150 (1998); S. Kumano and T.-H. Nagai, J. Comput. Phys. **201**, 651 (2004).
[51] R. K. Ellis, W. J. Stirling, and B. R. Webber, *QCD and Collider Physics* (Cambridge University Press, New York, 1996).
[52] P. J. Sutton, A. D. Martin, R. G. Roberts, and W. J. Stirling, Phys. Rev. D **45**, 2349 (1992).
[53] C.-G. Duan, N. Liu, and Z.-Y. Yan, Eur. Phys. J. C **50**, 585 (2007).
[54] M. Hirai, S. Kumano, and N. Saito, Phys. Rev. D **69**, 054021 (2004); **74**, 014015 (2006).
[55] M. Hirai, S. Kumano, T.-H. Nagai, and K. Sudoh, Phys. Rev. D **75**, 094009 (2007); M. Hirai, S. Kumano, M. Oka, and K. Sudoh, arXiv:0708.1816 [hep-ph] (Phys. Rev. D, in press).
[56] J. Pumplin, D. Stump, R. Brock, D. Casey, J. Huston, J. Kalk, H. L. Lai, and W. K. Tung, Phys. Rev. D **65**, 014013 (2002); JHEP 07 (2002) 012; A. D. Martin *et al*., Eur. Phys. J. C **28**, 455 (2003); **35**, 325 (2004).
[57] K. Prytz, Phys. Lett. **B311**, 286 (1993).
[58] A. Deshpande, R. Milner, R. Venugopalan, and W. Vogelsang, Annu. Rev. Nucl. Part. Sci. **55**, 165 (2005).
[59] http://casa.jlab.org/research/elic/elic.shtml.
[60] Our NPDF codes can be obtained from http://research.kek.jp/people/kumanos/nuclp.html.
[61] J. Arrington *et al*., J. Phys. Conf. Ser. **69**, 012024 (2007).
[62] For the MINERνA project, see http://minerva.fnal.gov/.
[63] S. Kumano, AIP Conf. Proc. **721**, 29 (2004).
[64] P04 proposal at http://j-parc.jp/NuclPart/Proposal_e.html; S. Kumano, Nucl. Phys. **A782**, 442 (2007).
[65] P906 proposal at http://p25ext.lanl.gov/e866/e866.html.
[66] http://www.gsi.de/fair/index_e.html.
[67] S.-Y. Li and X.-N. Wang, Phys. Lett. **B527**, 85 (2002).
[68] B. Z. Kopeliovich and A. V. Tarasov, Nucl. Phys. **A710**, 180 (2002).
[69] L. Frankfurt *et al*., JHEP 08 (2003) 043.
[70] G. Fai, J. Qiu, and X. Zhang, Phys. Rev. C **71**, 014901 (2005).
[71] F. Arleo and T. Gousset, arXiv:0707.2944 [hep-ph].
[72] K. Tywoniuk *et al*., Phys. Lett. **B657**, 170 (2007).
[73] B. Badelek and J. Kwiecinski, Phys. Rev. D **50**, R4 (1994).
[74] V. R. Zoller, Z. Phys. C **54**, 425 (1992).
[75] V. Barone *et al*., Z. Phys. C **58**, 541 (1993).
[76] W. Melnitchouk and A. W. Thomas, Phys. Rev. D **47**, 3783 (1993); W. Melnitchouk, A. W. Schreiber, and A. W. Thomas, Phys. Lett. **B335**, 11 (1994).
[77] G. Piller, W. Ratzka, and W. Weise, Z. Phys. A **352**, 427 (1995).